frontiers | Frontiers in Physics

TYPE Original Research
PUBLISHED 16 January 2023
DOI 10.3389/fphy.2022.1090437

OPEN ACCESS

EDITED BY
Luhong Mao,
Tianjin University, China

REVIEWED BY
Lei Duan,
Engineering Laboratory of Advanced Energy Materials, Ningbo Institute of Materials Technology and Engineering (CAS), China
Yue Su,
Chinese Academy of Sciences (CAS), China

*CORRESPONDENCE
Lin Chen,
chenlin@issp.ac.cn
Xingyou Tian,
xytian@issp.ac.cn

SPECIALTY SECTION
This article was submitted to Optics and Photonics, a section of the journal Frontiers in Physics

RECEIVED 05 November 2022
ACCEPTED 29 December 2022
PUBLISHED 16 January 2023

CITATION
Zhang L, Yang S, Xiao M, Chen L, Sun J, Ding J, Li X, Gong Y, Zheng K, Zhang X and Tian X (2023), Effect of Bi-B-Si-Zn-Al glass additive on the properties of low-temperature sintered silicon carbide ceramics.
Front. Phys. 10:1090437.
doi: 10.3389/fphy.2022.1090437

Effect of Bi-B-Si-Zn-Al glass additive on the properties of low-temperature sintered silicon carbide ceramics

Lan Zhang[1,2], Shuquan Yang[1,2], Meihui Xiao[1,2], Lin Chen[1,3]*, Jun Sun[1,3,4], Jianjun Ding[1,3], Xiaoxiao Li[1,3], Yi Gong[1,3], Kang Zheng[1,3], Xian Zhang[1,3] and Xingyou Tian[1,3]*

[1]Institute of Solid State Physics, Hefei Institutes of Physical Science, Chinese Academy of Sciences, Hefei, China, [2]University of Science and Technology of China, Hefei, China, [3]Key Lab of Photovoltaic and Energy Conservation Materials, Chinese Academy of Sciences, Hefei, China, [4]Lu'an Branch, Anhui Institute of Innovation for Industrial Technology, Lu'an, China

In this study, the performance of low-temperature sintered Bi-B-Si-Zn-Al glass/SiC composites by vacuum hot-press sintering between 700°C and 1000°C was investigated. The specimen had a relatively preferable density of 95.5% and thermal conductivity of 8.660 $Wm^{-1}K^{-1}$ after sintering at 900°C for 2 h. The dielectric constant and dielectric loss tangle of the composite were 32.9 and 0.57 at 20 GHz, respectively. The XRD analysis indicated the formation of Bi, Zn and $ZnAl_2O_4$ crystals, and the microstructure showed the low contact angle of the glass and SiC grain. Such low-temperature sintered SiC ceramic may have a promising application in the electronic field.

KEYWORDS

SiC ceramics, liquid phase sintering, LTCC, thermal conductivity, BBSZA glass

1 Introduction

LTCC (low-temperature co-fired ceramics), a technology developed from high-temperature co-fired ceramics (HTCC) multilayer circuits, has been widely used as the substrate for integrated device packaging. With the development of electronic equipment toward miniaturization and multi-function, the low thermal conductivity of LTCC becomes the limiting factor for its extensive application. In order to be co-fired with high electrical conductivity metals (Ag, Cu, and Au), the sintering temperatures of LTCC generally are required to be below 1,000°C. The restricted condition makes improving the thermal property of LTCC an urgent challenge. Silicon carbide (SiC) ceramic is an important structural material applied in mechanical seals, wear linings, and heat exchangers, owing to its excellent properties, such as high thermal conductivity(260–420$Wm^{-1}K^{-1}$) [1–3], abrasive resistance and hardness [4–6], appropriate thermal shock, and a low coefficient of thermal expansion similar to that of silicon [7–9]. However, the low self-diffusion of SiC ceramic caused by its stable Si-C covalent bonds makes densification sintering difficult without sintering additives.

The most prevailing method to densify SiC ceramics is by adding sintering additives.

These aids, together with SiO_2 adsorbed on the SiC particle surface [10], can transform into a liquid phase at a temperature lower than that of solid-state sintering of SiC. Alumina and rare earth (RE) oxides are popular combinations as aids to liquid phase sinter SiC ceramics, such as

TABLE 1 Additives, sintering temperature, relative density, thermal conductivity, and hardness of the SiC composites reported in the literatures.

Additive	Sintering temperature(°C)	Relative density (%)	Thermal conductivity ($Wm^{-1}K^{-1}$)	Hardness	Reference
Al_2O_3–Y_2O_3	1900	97	70	—	[30]
Al_2O_3–CeO_2	1840	99.1	—	—	[19]
A_lN–Y_2O_3–Sc_2O_3	1950	96.7	110.3	25 GPa	[31]
Y_2O_3–Sc_2O_3–MgO	1850	99.9	99	25.4 GPa	[32]
Al_2O_3–Y_2O_3–TiO_2	1900	96.2%	—	24.4 GPa	[21]
$Al2O_3$–Y_2O_3–CeO_2–MgO	1900	99.6%	73	28.1 GPa	[22]
$(Hf_{0.2}Mo_{0.2}Ta_{0.2}Nb_{0.2}Ti_{0.2})$ B_2	1900	99.3	—	21.9 GPa	[23]
ZnO–CaO–Al_2O_3–SiO_2 glass	1,550	95.5	7.104	1084HV10	[24]
This work	900	95.5	8.660	330HV	

Al_2O_3–Y_2O_3 [11–14], AlN–Er_2O_3 [15, 16], AlN–Sm_2O_3 [17, 18], and Al_2O_3–CeO_2 [19]. In recent years, researchers have been actively searching for new sintering additives, such as RE-Si-C (RE = La, Ce, and Pr) [20], TiO_2–SiC–Al_2O_3–Y_2O_3 [21], AlN–Y_2O_3–CeO_2–MgO (22), and $Hf_{0.2}Mo_{0.2}Ta_{0.2}Nb_{0.2}Ti_{0.2}$ [22]. Table 1 shows the relative density, thermal conductivity, and hardness of some liquid phase sintering SiC composites for comparison with this study. However, the liquid phase formation temperature of these additives always exceeds 1,500°C, which makes SiC ceramics not available in connecting with some low melting point metals, such as silver (961°C) and copper (1,083°C). Glass is a good choice to lower the sintering temperature of ceramics below 1,000°C [28, 29]. Low-temperature co-fired ceramics (LTCC) are most likely made up of alumina and glass [30]. However, little research has been conducted on replacing alumina with silicon carbide, although the thermal conductivity of SiC ceramic is tens of times higher than that of Al_2O_3 ceramic [31]. In this study, we use Bi–B–Si–Zn–Al (BBSZA) glass as the sintering aid to densify SiC ceramics. The BBSZA glass has a low melting point, good wettability with ceramics, and a thermal coefficient similar to that of silicon, which is a good choice applied as a sintering additive of ceramics [32]. In our research, the high thermal conductivity of 8.660 $Wm^{-1}K^{-1}$ is obtained by loading 50wt% BBSZA glass with SiC ceramics. The result shows the perspective of liquid phase sintered SiC ceramic applied in the low-temperature co-fired ceramics.

2 Experiment

The Bi_2O_3–B_2O_3–SiO_2–ZnO–Al_2O_3 glass is composed of 27 mol% Bi_2O_3 (Aladdin, 99.9%), 27 mol% ZnO (Aladdin, 99%), 26 mol% B_2O_3 (Aladdin, 98%), 15 mol% SiO_2(Aladdin, 99.99%), and 5 mol% Al_2O_3(Aladdin, 99.99%). The starting materials were mixed according to the proportion and melted at 1,150°C, thus quenched in deionized water and ground to a certain size (d_{50} = .29 μm). Here, 50-wt% SiC ceramics (Sinopharm; 99.8%, 0.8 μm) and 50-wt% BBSZA glass were mixed in ethanol and ball-milled in agate jars for 4 h at 350 rpm. After ball mixing, the slurry was dried at 60 °C for 12 h. Then, the dried powders were further ground in a mortar to avoid agglomeration. Finally, these powders were put into a graphite mold, which was padded with the graphite paper in the location of contact with powders and also sprayed with boron nitride on the inner wall of the mold. Then, the graphite mold was placed in a vacuum quartz tube furnace for sintering. The samples were heated in the hot-pressing furnace at a heating rate of 10°C min^{-1}under a uniaxial load of 30°Mpa. Table 2 lists the samples characterized in the study, as well as their composition and sintering temperature. Four sintering temperatures of 700°C, 800°C, 900°C, and 1,000°C, respectively, were set and kept for 1 h, marked as HP700, HP800, HP900, and HP1000, respectively.

The phase compositions of the samples were identified *via* an X-ray diffractometer (XRD, Rigaku SmartLab 9kW, Japan) with Cu Kα radiation (λ = .15418 nm). The microstructure of composites coated with Pt was observed by scanning electron microscopy (GeminiSEM 500, Germany). The bulk densities were determined using a multifunction densimeter (AR-150PM, China). The thermal conductivities were obtained using the hot disk thermal constant analyzer (TPS2200, Sweden). The dielectric properties were tested by using the vector network analyzer (MS46322B). Vickers hardness was measured by the Vickers hardness tester (HUAYIN, China), and each sample was tested five times to take the average value. The dc resistivities of samples were measured using a high-resistance meter (Tonghui, TH2683A, China) with an applied voltage of 10 V, and the dc resistivity of each sample was calculated using the following equation:

$$\rho = RS/L. \quad (1)$$

In the equation, ρ is on behalf of resistivity and R, S, and L represent the resistance, cross-sectional area, and the wire length of the sample, respectively.

3 Results and discussions

3.1 Phase composition

Figure 1D shows the XRD patterns of the SiC/BBSZA composites sintered at different temperatures. The XRD peaks of 6H-SiC (PDF#97-001-5325) and Bi (PDF#97-005-3797) were observed in all specimens. The presence of bismuth indicated that bismuth

TABLE 2 Batch composition and sintering temperature of SiC/BBSZA glass composites.

Sample	Batch composition (wt.%)	Sintering temperature (°C)
HP700	50 wt.% +50 wt.% SiC	700
HP800	50 wt.% +50 wt.% SiC	800
HP900	50 wt.% +50 wt.% SiC	900
HP1000	50 wt.% +50 wt.% SiC	1,000

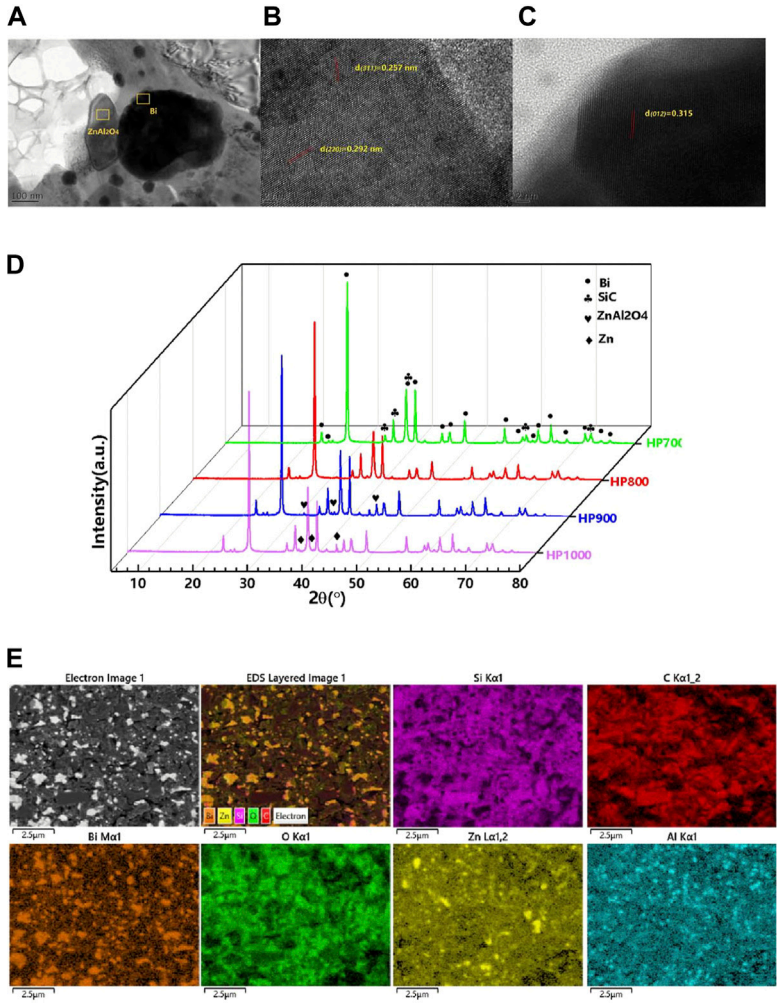

FIGURE 1
Phase composition. **(A)** Transmission electron microscopy (TEM) image of the SiC/BBSZA composites sintered at 900°C. **(B)** High-resolution TEM (HRTEM) image of $ZnAl_2O_4$. The d-spacing of .257 nm and .292 nm correspond to the d (311) and d (220) of $ZnAl_2O_4$. **(C)** High-resolution TEM (HRTEM) image of Bi. The d-spacing of .315 nm corresponds to d (012) of Bi. **(D)** X-ray diffraction (XRD) patterns of SiC/BBSZA composites sintered at 700°C, 800°C, 900°C, and 1,000°C, respectively. **(E)** EDS images of HP900.

oxide had been reduced. It is known that silicon carbide can reduce some metal oxides at high temperatures [33]. In this system, the following chemical reaction occurred:

$$SiC + Bi_2O_3 = Bi + SiO_2 + CO \uparrow . \quad (2)$$

This explains the appearance of bismuth. The phase with relatively small intensities of zinc was detected by XRD in the specimens of HP900 and HP1000. The emergence of zinc may be attributed to the decomposition of zinc oxide in the BBSZA glass. According to the Ellingham diagram, zinc oxide can decompose into zinc and oxygen under a certain ultra-low oxygen partial pressure (almost vacuum conditions) above 800°C. It can be comprehended that why the samples of HP700 and HP800 did not contain zinc. The chemical reaction process exhibits as following:

$$ZnO = Zn + O_2 \uparrow \quad (3)$$

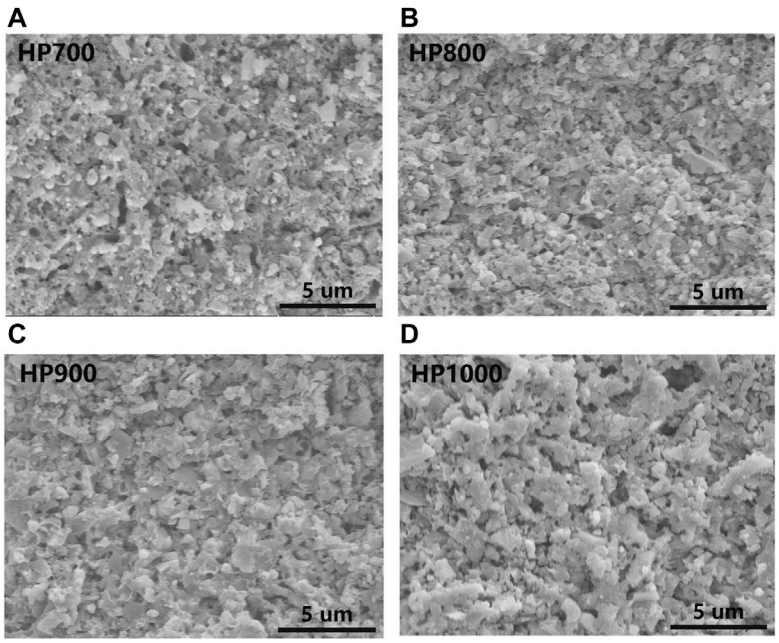

FIGURE 2
SEM images of SiC/BBSZA composites sintered at different temperatures: **(A)** 700°C, **(B)** 800°C, **(C)** 900°C, and **(D)** 1,000°C.

Moreover, aluminum oxide and zinc oxide in the BBSZA glass can react with each other to form spinel in the following reaction:

$$ZnO + Al_2O_3 = ZnAl_2O_4 \quad (4)$$

The X-ray feature peaks of $ZnAl_2O_4$ (PDF#97-000-9559) can be found in samples of HP800 and HP900. The crystal of $ZnAl_2O_4$ in HP1000 disappears due to the difference in Gibbs free energy between reactions (3), (4). The Gibbs free energy of reaction (3) is lower than that of reaction (4), which makes reaction (3) have more chance to occur at 1,000°C.

A high-resolution transmission electron microscope (HRTEM) can determine the phase of composites by analyzing the diffraction patterns and streaks. Figure 1A shows the HRTEM images of the SiC/BBSZA composite ceramic sintered at 900°C. The interplanar spacing values of .257 nm and .292 nm correspond to d (311) and d (220) of $ZnAl_2O_4$, respectively, as shown in Figure 1B. Otherwise, in Figure 1C, the interplanar spacing value of .315 nm matches d (012) of the Bi crystal. An amorphous phase can be seen around the $ZnAl_2O_4$ and Bi crystals, which represent the BBSZA glass. The analysis results of HRTEM verify the conclusion of XRD.

Figure 1E shows the EDS mapping images of the SiC–BBSZA composite ceramic sintered at 900°C. EDS mapping can exhibit the distribution of elements in the composites. The appearing location of the Si element matched well with that of the C element, indicating the existence of the SiC crystal in this area. It is worth noting that the O element almost has the same location as that of the Si and C elements. This could further prove the occurrence of reaction (2). In addition, the distribution of Bi, Zn, and Al elements is both uneven along with the phenomenon of aggregation. The aggregation of the Bi element is because of the generation of bismuth in reaction (2), and the aggregation of Zn and Al elements is contributed by the products of Zn and $ZnAl_2O4$ in reactions (3), (4). Otherwise, the position of Al element aggregation is partially the same as the Zn element, suggesting the formation of the $ZnAl_2O_4$ crystal. These EDS mapping images corresponded well with the results of XRD.

3.2 Microstructure

The microstructures of SiC/BBSZA composites sintered at different temperatures are shown in Figures 2A–D. The samples of HP700, HP800, and HP900 exhibited dense morphology except that the sample of HP700 formed some obvious pores, owing to the poor liquidity of glass at 700°C. The liquid phase sintering process could be divided into three stages: particle rearrangement, solution and precipitation, and solid-state sintering [34]. The densification of composites occurs quickly in the first stage as pores between grains are filled with the liquid phase. So, good flowability of the liquid phase facilitates the densification of ceramics. At 800°C–1000°C, the microstructure of samples showed homogeneous and dense morphology, which is beneficial to their thermal property. Nevertheless, HP1000 seems to have larger grains than other composites sintered at a lower temperature. So, we etched these composites with strong acids and alkalis to remove the glass, Bi, Zn, and $ZnAl_2O_4$; as shown in Figures 3A–D, the characteristic of acid and alkali resistance of SiC provides a convenient way to display the SiC grain size. It can be found that the distribution of SiC particle sizes is uneven. Also, compared with other samples, the number of fine grain particles of HP1000 decreased. This phenomenon can be attributed to the occurrence of secondary recrystallization [35]. As we all know, normal grain growth exhibits an increase in the average size, but if the grain boundaries are hindered by a second phase, such as impurities, the normal grain growth will stop. Secondary recrystallization is a process in which large grains grow excessively by consuming a uniform fine grain matrix that is essentially no longer growing. In particular, secondary recrystallization may occur when the

10.3389/fphy.2022.1090437

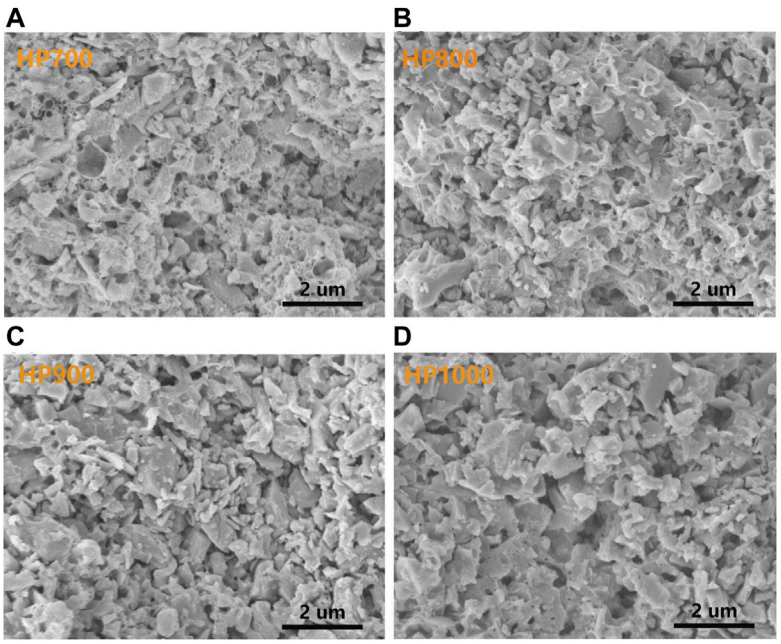

FIGURE 3
SEM images of SiC/BBSZA composites sintered at different temperatures etched with strong acids and alkalis: **(A)** 700°C, **(B)** 800°C, **(D)** 900°C, and **(D)** 1,000°C.

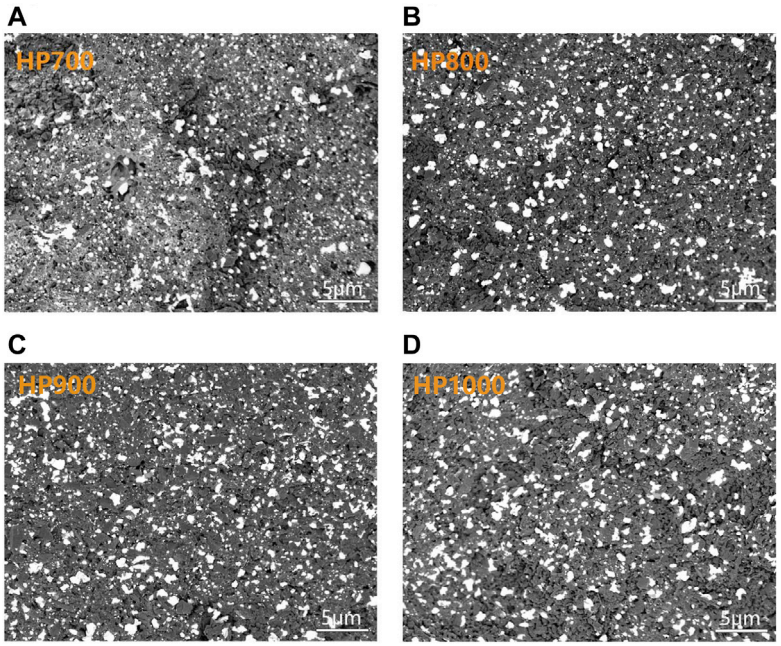

FIGURE 4
Backscattered electron (BSE) images of SiC/BBSZA composites sintered at different temperatures: **(A)** 700°C, **(B)** 800°C, **(C)** 900°C, and **(D)** 1,000°C.

particle size of the original material is not uniform or the sintering temperature is high. The driving force of secondary recrystallization is the excess interfacial energy of the grain boundary. The grain boundary phase of the large grains moves under the impetus of interfacial energy, resulting in large grains' further growth and small grains' disappearance. After secondary recrystallization occurs, the gas pores enter the grain interior and become isolated pores, making the sintering rate decrease or even stop. Because the

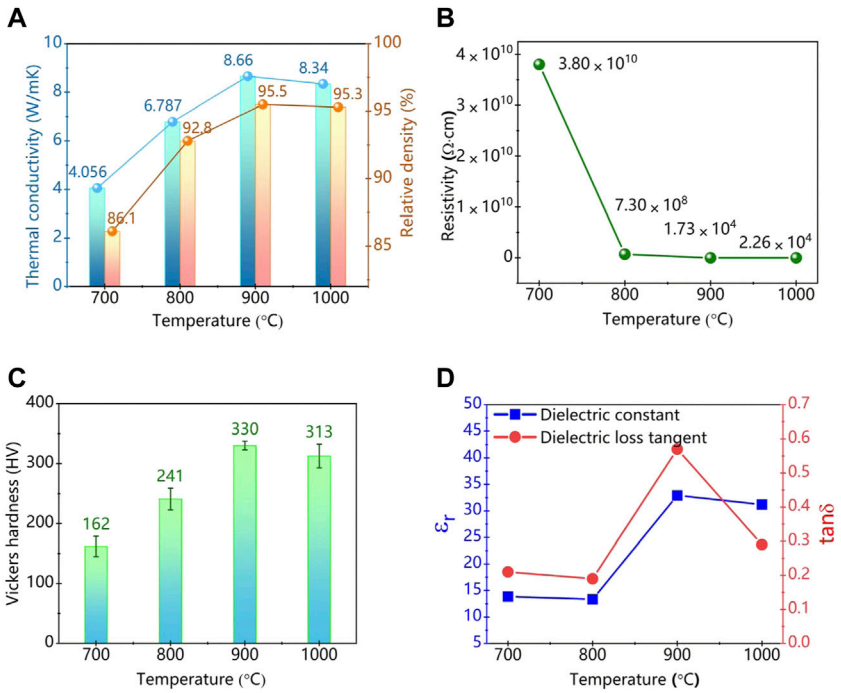

FIGURE 5
Thermal conductivity, resistivity, Vickers hardness, and dielectric properties of SiC/BBSZA composites sintered at different temperatures. **(A)** Thermal conductivity of SiC/BBSZA composites with different sintering temperatures; **(B)** DC resistivity of SiC/BBSZA composites with different sintering temperatures; **(C)** Vickers hardness of SiC/BBSZA composites with different sintering temperatures; **(D)** dielectric constant and dielectric loss tangent of SiC/BBSZA composites with different sintering temperatures.

pressure of the gas in the small pores is relatively large, it may migrate and diffuse into the large pores at low pressure, making the pores on the grain boundaries larger as the grains grow, i.e., the pore size increases.

Backscattered electron (BSE) images can clearly show the distribution of the different phases of the composites as the brightness of the lining depends on the atomic number. In this study, we take advantage of it to know the distribution of Bi, BBSZA glass, and SiC. Figures 4A–D show the microstructures of the ESB pattern of SiC/BBSZA composite ceramics sintered at different temperatures. The bright areas represent the location of the heavy atom in the samples (referring to Bi and BBSZA glass in this study), while the dark areas show the distribution of light atoms (referring to SiC, Zn, and $ZnAl_2O_4$ in the samples). The distribution of composites of HP800, HP900, and HP1000 in the bright regions both remained uniform. On the contrary, the HP700 sample exhibited uneven distribution in the bright areas due to the poor liquidity of glass. In addition, with the temperature increasing from 800°C to 900°C, the shape of light areas gradually tends to change from round to elongated, which indicated the flowability of Bi and BBSZA glass became better. This suggests the structure of the sample HP900 may be denser than that of HP700.

3.3 Thermal conductivity

Figure 5A shows the curves of relative density and thermal conductivity of SiC/BBSZA composites sintered at different temperatures. The two curves showed a similar trend, which both increased as the sintering temperature increased up to 900°C and then decreased. The thermal conductivity of composites is closely related to the density in liquid phase sintering because pores can impede the propagation of phonons. With the sintering temperature increasing from 700°C to 900°C, the thermal conductivity of the composites varied from 4.056 $Wm^{-1}K^{-1}$ to 8.660 $Wm^{-1}K^{-1}$; meanwhile, the relative density increased from 86.1% to 95.5%. The thermal conductivity of the SiC/BBSZA composites reached the highest (8.66 $Wm^{-1}K^{-1}$) at 900°C, which outdistances that of conventional LTCC (~2–4 $Wm^{-1}K^{-1}$). In addition, the thermal conductivity decreased by 3.7% when the sintering temperature varied from 900°C to 1,000°C. There may be two reasons for the decrease in thermal conductivity of HP1000. The first factor is the decrease in the relative density, which may be caused by the increase in pore size. The other factor may be the disappearance of $ZnAl_2O_4$ at 1,000°C. After all, the thermal conductivity of $ZnAl_2O_4$ potentially is higher than that of Al_2O_3 [36–38], which is a good thermal conductor in composites.

3.4 DC resistivity

Figure 5B shows the electric resistivities of SiC/BBSZA composites sintered at different temperatures. The resistivities decreased sharply when the temperature varied from 700°C to 900°C and then have a small rise at 1,000°C. According to the pseudo-percolation model [39], electrons of the composite tend to conduct along the lowest resistance (the thinnest grain boundary).

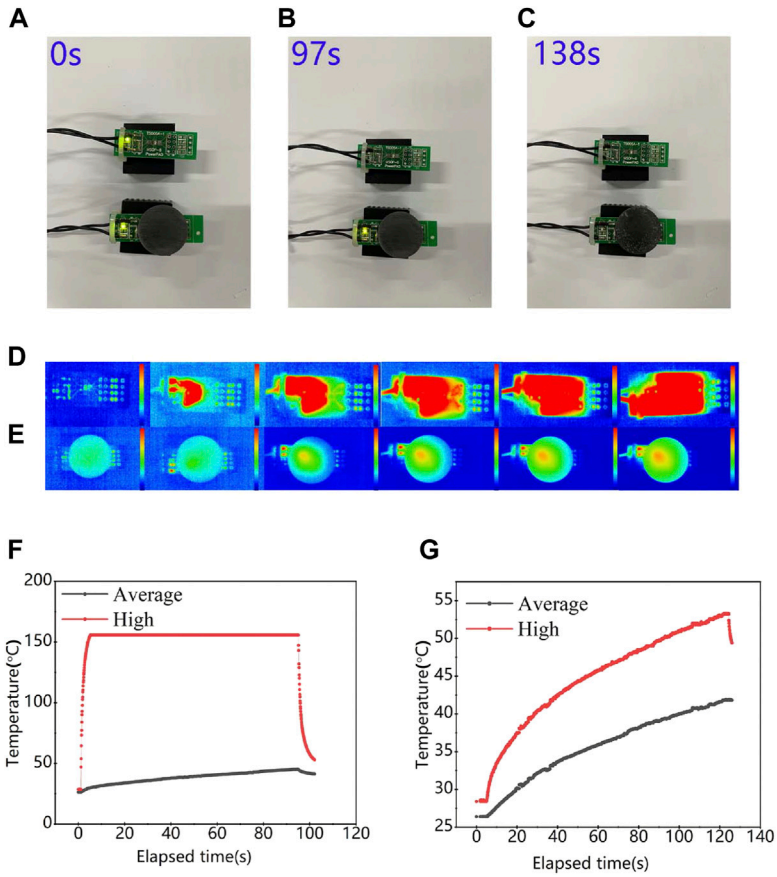

FIGURE 6
Comparison of heat dissipation performance with and without HP900 in the chip resistor. **(A–C)** Optical images of the electronic device with and without HP900 as the heat dissipating material; **(D,E)** Corresponding infrared thermal images of working electronic devices with and without HP900 as the heat dissipating material; **(F,G)** maximum and average temperatures of two chip resistors as a function of their operation time.

Bismuth has a certain electrical conductivity due to its metallicity. The abundant SiC and bismuth could touch each other to form a conductive network, which is beneficial to electron conduction. So, the density microstructure and uniform distribution of bismuth are the main reasons why the HP900 sample has the lowest resistivity. Otherwise, the high resistivities of HP700 and HP800 samples could be attributed to two reasons: first, the amorphous phase (BBSZA glass), an insulator, hinders electron conduction; second, pores in the composites destroy the contact of SiC particles.

3.5 Hardness

Figure 5C shows the Vickers hardness of SiC/BBSZA composites sintered at different temperatures. The factors influencing the hardness of materials include the microstructure, composition, crystallographic direction, and grain size. The grain size of SiC/BBSZA composites does not change much when the sintering temperatures are between 700°C and 900°C. Therefore, the difference in the microstructure of these samples may play a vital role in hardness. The hardness showed an increasing trend with the rising temperature, similar to that of relative density. The hardness of the composites of HP900 is the highest up to 330 HV, which corresponds to the densest structure of composites at the sintering temperature. The decrease in pores enhances the hardness of materials. However, hardness tends to decrease when the pore size becomes bigger. This can interpret the decreasing hardness of HP1000 [40].

3.6 Dielectric properties

Figure 5D shows the curves of the dielectric constant and the dielectric loss tangent of SiC/BBSZA composites with different sintering temperatures at 20 GHz. It can be observed that the dielectric constant and dielectric loss tangent represented a similar trend, in which both increased when the temperature varied from 700°C to 900°C and then decreased. The following formula is used for calculating the permittivity of complexes—Lichtenecker's logarithmic mixture law [41–43]:

$$In\varepsilon = \sum_{i=0}^{n} V_i In\varepsilon_i, \quad (5)$$

where ε represents the permittivity of composites, ε_i is on behalf of the permittivity of each component in the sample, and V_i represents the volume fraction occupied by each component, and $\sum V_i = 1$. In this composite, the dielectric constant can be presented using this law, and let us take HP900 as an example.

$$In\varepsilon = V_{SiC}In\varepsilon_{SiC} + V_{Bi}In\varepsilon_{Bi} + V_{glass}In\varepsilon_{glass} + V_{SiO2}In\varepsilon_{SiO2} + V_{ZnAl2O4}In\varepsilon_{ZnAl2O4} + V_{Zn}In\varepsilon_{Zn} + V_{pores}In\varepsilon_{pores}. \quad (6)$$

By searching the literature, it is found that the dielectric constants of 6H-SiC, Bi, $ZnAl_2O_4$, and Zn are approximately 6.7, 3.3, 8.5, and 2.1, respectively [44–46]. It is essential to note that the dielectric constant of pores is low to 1.0, the same as that of air. The sample of HP900 obtained the biggest dielectric constant because the composite has fewer pores than other samples. Moreover, the disappearance of $ZnAl_2O_4$ and the increase of Zn lead the dielectric constant of the composite of HP1000 to decrease even though the sample had a dense structure. Otherwise, the dielectric loss has a close relationship with electrical conductivity because the electric energy can be converted into heat. It can be understood that better electrical conductivity leads to a higher dielectric loss tangent. Accordingly, the resistances' variation trend of composites sintered at different temperatures is almost the same as that of the dielectric loss tangent; the sample of HP900 holding the smallest resistivity had the biggest dielectric loss tangent, which conforms to the previous rule.

3.7 Heat dissipation performance

To verify the thermal property of SiC/BBSZA composites sintered at 900°C, we fasten the sample on a chip resistor (JUC-31F) to observe its effect on device heat dissipation, simultaneously using another resistor as a blank control group to compare. The chip resistor can automatically power off when its temperature reaches to a certain value. From Figures 6A–C, it was found that the sintered sheet of HP900 can improve the heat dissipation performance of chip resistors as it can prolong the LED lighting time by nearly 50% more than that of the blank group. The infrared thermal imaging camera was used to record the temperature change of two chip resistors during the heating process, as shown in Figures 6D, E. The composites can effectively hinder the rapid rise of temperature of the device, owing to its high thermal conductivity. The curves of the average and maximum temperature of the two group devices during the heating process are shown in Figures 6F, G. The maximum temperature of the blank group rose to 158°C in a few seconds, while the device possessing composites varied from 27°C to 53°C in 120 s. Moreover, the curves of the highest and average temperature in the chip having composites are closer than that of the blank group. These differences between the two groups suggest the excellent thermal property of SiC/BBSZA composites sintered at 900°C.

4 Conclusion

In this research, the effect of sintering temperatures on densification and properties of SiC/BBSZA composite ceramics are investigated, and these are the obtained results:

- XRD, TEM, and EDS analysis results suggested the formation of Bi, Zn, and $ZnAl_2O_4$ crystals in the composites, which can contribute to thermal conductivity and has a vital influence on other properties of samples.
- The SiC/BBSZA composite sintered at 900°C showed the highest thermal conductivity value (8.660 $Wm^{-1}K^{-1}$), suitable dielectric constant (ε = 32.9), dielectric loss (tanð = .57), Vickers hardness (330 HV), and dc resistivity (1.71 × 104 Ω cm), which maybe has good application prospects for electronic substrate materials due to its low sintering temperature and excellent comprehensive performance.
- The decrease in the relative density of the composite sintered at 1,000°C may be attributed to the occurrence of secondary recrystallization, and the SEM of composites etched with strong acids and alkalis also supported the explanation.

Data availability statement

The original contributions presented in the study are included in the article/Supplementary Material; further inquiries can be directed to the corresponding authors.

Author contributions

LZ, LC, and XT contributed to the conception and design of the study. LZ and LC performed the statistical analysis. LZ wrote the first draft of the manuscript. All authors contributed to the manuscript revision, read, and approved the submitted version.

Funding

This work was supported by the CASHIPS Director's Fund (No. YZJJZX202015) and the Anhui Science and Technology Major Project (No. 202103a05020014).

Conflict of interest

The authors declare that the research was conducted in the absence of any commercial or financial relationships that could be construed as a potential conflict of interest.

Publisher's note

References

1. Slack GA. Nonmetallic crystals with high thermal-conductivity. *J Phys Chem Sol* (1973) 34(2):321–35. doi:10.1016/0022-3697(73)90092-9

2. Kawamura T, Hori D, Kangawa Y, Kakimoto K, Yoshimura M, Mori Y. Thermal conductivity of SiC calculated by molecular dynamics. *Jpn J Appl Phys* (2008) 47(12): 8898–901. doi:10.1143/jjap.47.8898

3. Yamada I, Kume S, Nakano H, Watari K, editors *Macro- and micro-scale thermal conductivities of SiC single crystal and ceramic*. In: 2nd International Symposium on SiAIONs and Non-Oxides; 2009 Dec 02-05; Mie, Japan (2009).

4. Hirai T, Niihara K. Hot hardness OF SIC single-crystal. *J Mater Sci* (1979) 14(9): 2253–5. doi:10.1007/bf00688433

5. Ma ZY, Bi J, Lu YX, Shen HW, Gao YX. Abrasive wear of discontinuous SIC reinforced aluminum-alloy composites. *Wear* (1991) 148(2):287–93. doi:10.1016/0043-1648(91)90290-b

6. Xiao P, Li Z, Zhu Z, Xiong X. Preparation, properties and application of C/C-SiC composites fabricated by warm compacted-*in situ* reaction. *J Mater Sci Tech* (2010) 26(3): 283–8. doi:10.1016/s1005-0302(10)60047-3

7. Park K, Vasilos T. Interface and thermal shock resistance of SiC fiber/SiC composites. *Scripta Materialia* (1998) 39(11):1593–8. doi:10.1016/s1359-6462(98)00356-x

8. Yin XW, Cheng LF, Zhang LT, Xu YD. Thermal shock behavior of 3-dimensional C/SiC composite. *Carbon* (2002) 40(6):905–10. doi:10.1016/s0008-6223(01)00225-1

9. Yang Z, He X, Wang L, Liu R, Hu H, Wang L, et al. Microstructure and thermal expansion behavior of diamond/SiC/(Si) composites fabricated by reactive vapor infiltration. *J Eur Ceram Soc* (2014) 34(5):1139–47. doi:10.1016/j.jeurceramsoc.2013.10.038

10. Yoshimura M, Kase JI, Somiya S. Oxidation of SiC powder by high-temperature, high-pressure H2O. *J Mater Res* (1986) 1(1):100–3. doi:10.1557/jmr.1986.0100

11. Gomez E, Echeberria J, Iturriza I, Castro F. Liquid phase sintering of SiC with additions of Y2O3, Al2O3 and SiO2. *J Eur Ceram Soc* (2004) 24(9):2895–903. doi:10.1016/j.jeurceramsoc.2003.09.002

12. Huang R, Gu H, Zhang JX, Jiang DL. Effect of Y2O3-Al2O3 ratio on inter-granular phases and films in tape-casting alpha-SiC with high toughness. *Acta Materialia* (2005) 53(8):2521–9. doi:10.1016/j.actamat.2004.10.055

13. Wang G, Krstic VD. Effect of Y2O3 and total oxide addition on mechanical properties of pressureless sintered beta-SiC. *J Mater Sci Tech* (2003) 19(3):193–6.

14. Roman-Manso B, Chevillotte Y, Osendi MI, Belmonte M, Miranzo P. Thermal conductivity of silicon carbide composites with highly oriented graphene nanoplatelets. *J Eur Ceram Soc* (2016) 36(16):3987–93. doi:10.1016/j.jeurceramsoc.2016.06.016

15. Guo SQ, Hirosaki N, Tanaka H, Yamamoto Y, Nishimura T. Oxidation behavior of liquid-phase sintered SiC with AlN and Er2O3 additives between 1200 °C and 1400 °C. *J Eur Ceram Soc* (2003) 23(12):2023–9. doi:10.1016/s0955-2219(03)00030-x

16. Kim YW, Chun YS, Nishimura T, Mitomo M, Lee YH. High-temperature strength of silicon carbide ceramics sintered with rare-earth oxide and aluminum nitride. *Acta Materialia* (2007) 55(2):727–36. doi:10.1016/j.actamat.2006.08.059

17. Balog M, Sajgalik P, Hnatko M, Lences Z, Monteverde E, Keckes J, et al. Nano-versus macro-hardness of liquid phase sintered SiC. *J Eur Ceram Soc* (2005) 25(4):529–34. doi:10.1016/j.jeurceramsoc.2004.01.026

18. Taguchi SP, Balestra RM, Garcia GCR, Ribeiro S. Spontaneous infiltrations of compound systems of Y2O3, Sm2O3, RE2O3, Al2O3 and AIN in SiC ceramics. *Ceram Int* (2010) 36(1):9–14. doi:10.1016/j.ceramint.2009.05.041

19. Liang HQ, Yao XM, Zhang JX, Liu XJ, Huang ZR. Low temperature pressureless sintering of alpha-SiC with Al2O3 and CeO2 as additives. *J Eur Ceram Soc* (2014) 34(3): 831–5. doi:10.1016/j.jeurceramsoc.2013.09.015

20. Xu K, Chang KK, Zhou XB, Chen LL, Liu JW, Deng ZX, et al. Thermodynamic descriptions of the light rare-earth elements in silicon carbide ceramics. *J Am Ceram Soc* (2020) 103(6):3812–25. doi:10.1111/jace.17031

21. Khodaei M, Yaghobizadeh O, Ehsani N, Baharvandi HR, Dashti A. The effect of TiO2 additive on sinterability and properties of SiC-Al2O3-Y2O3 composite system. *Ceram Int* (2018) 44(14):16535–42. doi:10.1016/j.ceramint.2018.06.073

22. Yuan JH, Guo WM, Liu Y, Sun SK, Duan XM, Jia DC, et al. Hardness and toughness improvement of SiC-based ceramics with the addition of (Hf0.2Mo0.2Ta0.2Nb0.2Ti0.2)B-2. *J Am Ceram Soc* (2022) 105(3):1629–34. doi:10.1111/jace.18209

23. Volz E, Roosen A, Hartung W, Winnacker A. Electrical and thermal conductivity of liquid phase sintered SiC. *J Eur Ceram Soc* (2001) 21(10-11):2089–93. doi:10.1016/s0955-2219(01)00178-9

24. Cho T-Y, Kim Y-W, Kim KJ. Thermal, electrical, and mechanical properties of pressureless sintered silicon carbide ceramics with yttria-scandia-aluminum nitride. *J Eur Ceram Soc* (2016) 36(11):2659–65. doi:10.1016/j.jeurceramsoc.2016.04.014

25. Kim Y-H, Kim Y-W, Lim K-Y, Lee S-J. Mechanical and thermal properties of silicon carbide ceramics with yttria-scandia-magnesia. *J Eur Ceram Soc* (2019) 39(2-3):144–9. doi:10.1016/j.jeurceramsoc.2018.09.021

26. Kang ES, Kim YW, Lim KY, Lee SJ. New quaternary additive for processing fully ceramic microencapsulated fuels without applied pressure. *J Eur Ceram Soc* (2022) 42(4): 1238–48. doi:10.1016/j.jeurceramsoc.2021.12.026

27. Wang W, Teng YC, Zhao XF, Wang SL. ZCAS-assisting low-temperature hot-press sintering of SiC ceramic for immobilizing simulated radioactive graphite. *Ceram Int* (2020) 46(15):23406–16. doi:10.1016/j.ceramint.2020.06.110

28. Feng XY, Lv YY, Zhang L, Ge DW, Li XX, Sun J, et al. Effect of AlN addition on phase formation in the LTCC with Al2O3/AlN biphasic ceramics based on BBSZ glass. *Ceram Int* (2020) 46(10):16895–900. doi:10.1016/j.ceramint.2020.03.268

29. Lv YY, Zhang L, Yang SQ, Wang ZH, Chen L, Sun J, et al. Effect of graphene addition on a borosilicate glass/alumina composite for LTCC technology. *Ceram Int* (2021) 47(9): 13035–42. doi:10.1016/j.ceramint.2021.01.167

30. Xia Q, Zhong CW, Luo J. Low temperature sintering and characteristics of K2O-B2O3-SiO2-Al2O3 glass/ceramic composites for LTCC applications. *J Mater Sci-mater Electron* (2014) 25(10):4187–92. doi:10.1007/s10854-014-2147-0

31. Cho TY, Kim YW. Effect of grain growth on the thermal conductivity of liquid-phase sintered silicon carbide ceramics. *J Eur Ceram Soc* (2017) 37(11):3475–81. doi:10.1016/j.jeurceramsoc.2017.04.050

32. Zhang L, Yang SQ, Xiao MH, Chen L, Sun J, Ding JJ, et al. Influence of silicon carbide nanowires on the properties of Bi-B-Si-Zn-Al glass based low temperature co-fired ceramics. *Ceram Int* (2022) 48(17):25382–9. doi:10.1016/j.ceramint.2022.05.212

33. Lin HT, Becher PF. HIGH-TEMPERATURE creep deformation of alumina SIC-whisker composites. *J Am Ceram Soc* (1991) 74(8):1886–93. doi:10.1111/j.1151-2916.1991.tb07804.x

34. Jean JH, Gupta TK. Liquid-phase sintering in the glass-cordierite system: Particle size effect. *JOURNAL MATERIALS SCIENCE* (1992) 27:4967–73. doi:10.1007/bf01105262

35. German RM. Coarsening in sintering: Grain shape distribution, grain size distribution, and grain growth kinetics in solid-pore systems. *Crit Rev Solid State Mater Sci* (2010) 35(4):263–305. doi:10.1080/10408436.2010.525197

36. Roshni SB, Sebastian MT, Surendran KP. Can zinc aluminate-titania composite be an alternative for alumina as microelectronic substrate? *Scientific Rep* (2017) 7:40839. doi:10.1038/srep40839

37. Surendran KP, Sebastian MT, Manjusha MV, Philip J. A low loss, dielectric substrate in ZnAl2O4-TiO2 system for microelectronic applications. *J Appl Phys* (2005) 98(4): 044101. doi:10.1063/1.2007873

38. Lan XK, Li J, Zou ZY, Xie MQ, Fan GF, Lu WZ, et al. Improved sinterability and microwave dielectric properties of Zn0.5Ti0.5 (3+)-doped ZnAl2O4 spinel solid solution. *J Am Ceram Soc* (2019) 102(10):5952–7. doi:10.1111/jace.16453

39. TabkhPaz M, Parmar K, Ali AM, Park S. Effects of foaming through leaching on the electrical behavior of polystyrene/carbon nanotube composites. *J Thermoplastic Compos Mater* (2016) 29(6):735–53. doi:10.1177/0892705714533375

40. Li ZY, Yang LL, Li Y, Yang YN, Zhou CH, Ding YB, et al. Effects of pore size on the mechanical properties of three-dimensionally ordered macroporous nickel. *Mater Des* (2013) 45:52–5. doi:10.1016/j.matdes.2012.09.009

41. Zakri T, Laurent JP, Vauclin M. Theoretical evidence for `Lichtenecker's mixture formulae' based on the effective medium theory. *J Phys D-Applied Phys* (1998) 31(13): 1589–94. doi:10.1088/0022-3727/31/13/013

42. Gao L, Gu JZ. Effective dielectric constant of a two-component material with shape distribution. *J Phys D-Applied Phys* (2002) 35(3):267–71. doi:10.1088/0022-3727/35/3/316

43. Goncharenko AV, Lozovski VZ, Venger EF. Lichtenecker's equation: Applicability and limitations. *Opt Commun* (2000) 174(1-4):19–32. doi:10.1016/s0030-4018(99)00695-1

44. Digregorio JF, Furtak TE. Raman-SCATTERING by surface PHONON-polaritons in large SIC microcrystals. *Solid State Commun* (1994) 89(2):163–6. doi:10.1016/0038-1098(94)90398-0

45. Animalu AOE. Electronic structure of transition metals. II. Phonon spectra. *Phys Rev B* (1973) 8(8):3555–62. doi:10.1103/physrevb.8.3555

46. Surendran KP, Santha N, Mohanan P, Sebastian MT. Temperature stable low loss ceramic dielectrics in (1-x)ZnAl $\mathsf{_{2}}$ O $\mathsf{_{4}}$ -xTiO $\mathsf{_{2}}$ system for microwave substrate applications. *Eur Phys J B* (2004) 41(3):301–6. doi:10.1140/epjb/e2004-00321-8